PROCEEDINGS OF SCIENCE

Radiation Hardness Challenges for Vertex Detection in the Future

Sally Seidel [a,*]

a Department of Physics and Astronomy, University of New Mexico, Albuquerque, NM, USA

E-mail: seidel@unm.edu

Radiation tolerance specifications for experiments at several future particle colliders are summarized. The role of tracking systems and timing systems in vertexing is emphasized, and so the consequences of radiation damage upon both types of systems are discussed. Challenges to vertexing that arise from radiation damage in semiconductor detectors are reviewed. Features observed in detector response at the highest controlled fluences are noted. Approaches to mitigate the effects of radiation damage and thereby achieve excellent tracking and timing are reviewed.

The 32nd International Workshop on Vertex Detectors (VERTEX2023)
16-20 October 2023
Sestri Levante, Genova, Italy

[*] Speaker

PoS(VERTEX2023)058

1. Colliders on the research horizon, and radiation environments foreseen for them

Experiments planned for the High-Luminosity Large Hadron Collider (HL-LHC) are anticipating operations under integrated fluence and dose conditions that were inconceivable only a few years ago. Integrated luminosities of 3 ab^{-1} at ATLAS and CMS, 50 fb^{-1} at LHCb, and, at ALICE, 5 fb^{-1}, are expected. Simulated conditions in ATLAS [1] (Figure 1) and CMS [2] (Figure 2) require experimenters to plan for fluences well beyond 10^{16} n_{eq}/cm^2 in the inner tracking and possibly in the timing detectors. At LHCb [3], challenges with high fluence will be exacerbated by non-uniform exposure. Figure 3 shows the annual high energy hadron fluence expected in the LHCb Mighty Tracker of the Upgrade II era. The maximum fluence at the center of that inner layer is anticipated to be 3 x 10^{14} n_{eq}/cm^2, and a safety factor of 2 should be applied to this in instrument design. The dose is expected to drop by a factor of about 6 between 5.1 and 12.5 mm from the beamline. This non-uniform exposure leads to challenges on high voltage tolerance, guard ring design, and technology to maintain full depletion with each sensor.

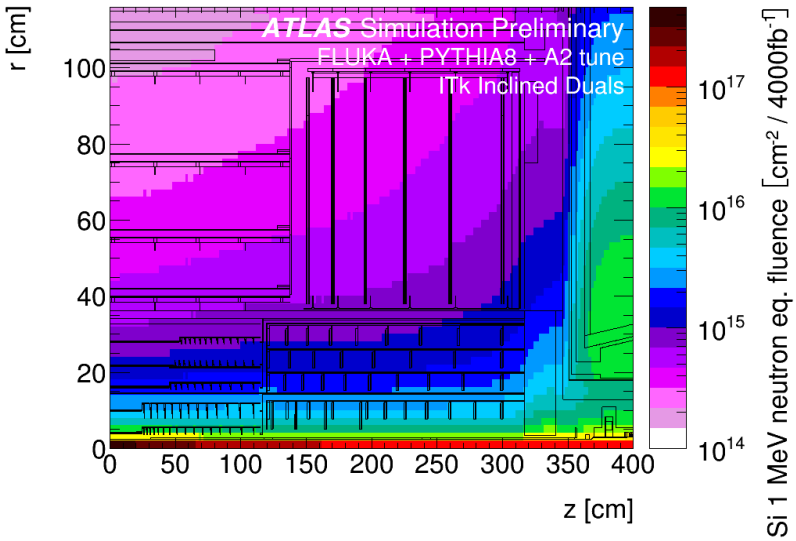

Fig. 1. Simulated 1 MeV neutron equivalent fluence per 4000 fb^{-1} of integrated luminosity in the ATLAS Inner Tracker ITK. Figure taken from [1].

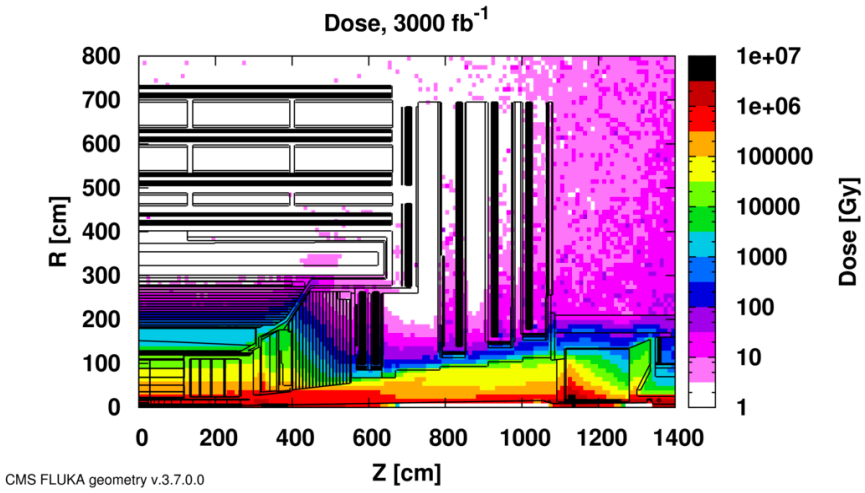

Fig. 2. Absorbed dose in the CMS cavern after an integrated luminosity of 3000 fb^{-1}. R is the transverse distance from the beamline and Z is the distance along the beamline from the interaction point at Z = 0. Figure taken from [2].

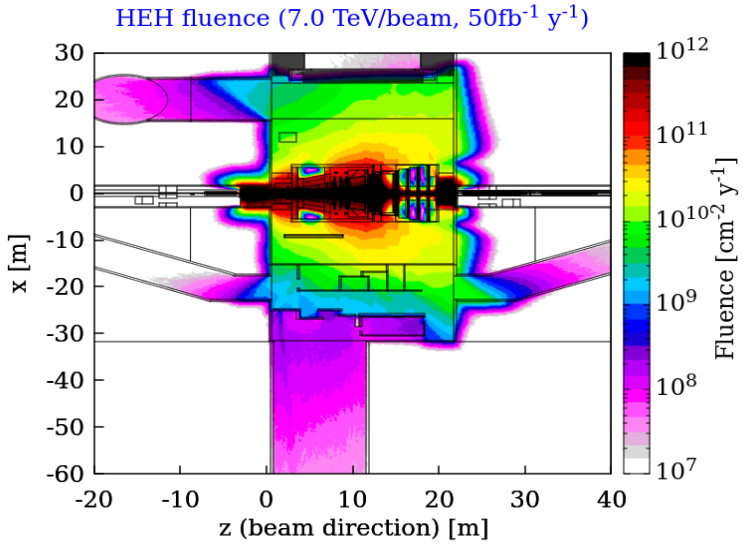

Fig. 3. Top view of annual high energy hadron fluence at the LHCb Mighty Tracker (averaged in the third dimension between -1.1 m and 1.1 m with respect to the beam height) during Run 5, assuming the same IR8 layout as in Run 3-4 and an annual luminosity of 50 fb^{-1}. The simulation assumed upward polarity of the LHCb spectrometer and an external horizontal crossing of 250 μrad, pointing inside the ring, at $\sqrt{s}$ = 14 TeV. Figure taken from [3].

In future experiments, vertexing will require simultaneous excellence in both position and timing measurements. Radiation challenges to the vertex detectors originate mostly with particles from the primary interaction point. Timing detectors, which are increasingly critical for identifying the vertex of interest by suppressing pile-up tracks, will be located relatively far from the primary vertex and thus subject to radiation with a different origin, for example calorimeter backsplash. The ATLAS High Granularity Timing Detector (HGTD) [4] will be located ±3.5 m from the interaction point, at radii from 120 to 640 mm. CMS will install Barrel Timing Layer (BTL) and Endcap Timing Layer (ETL) detectors [5], the latter of which will be located ±3.0 m from the interaction point and will span radii from 315 to 1200 mm. For the HGTD, at radius 120 mm, the predicted fluence is 5.6 x 10^{15} n_{eq}/cm^2 and the total ionizing dose (TID), 3.3 MGy.

ATLAS applies a safety factor of 1.5 on both of those estimates, and a second factor of 1.5 to the TID estimate to cover uncertainties in the behavior of the electronics after radiation, primarily for low-dose-rate effects. With these safety factors, the HGTD requirements are 8.3 x 10^{15} n_{eq}/cm^2 and 7.5 MGy. A minimum charge of 4 fC is needed for high efficiency signal collection. With existing technology, this level of charge collection can be achieved up to fluence 2.5 x 10^{15} n_{eq}/cm^2 and dose 2.0 MGy. Figure 4 shows the expected nominal fluence and ionizing dose as functions of the outermost sensor layer of the HGTD, for 4000 fb^{-1} integrated luminosity and before inclusion of safety factors. For the CMS BTL, the anticipated radiation exposure is 30 kGy and 1.9 x 10^{14} n_{eq}/cm^2, while for the ETL in the highest pseudorapidity (η) part of the endcap, the exposure will be 450 kGy and 1.6 x 10^{15} n_{eq}/cm^2. These numbers should be multiplied by a 1.5 safety factor, and of course the ASICs must be radiation tolerant and single event upset (SEU) compliant at the same fluence. Figure 5 shows the predicted dose profiles in the BTL and ETL.

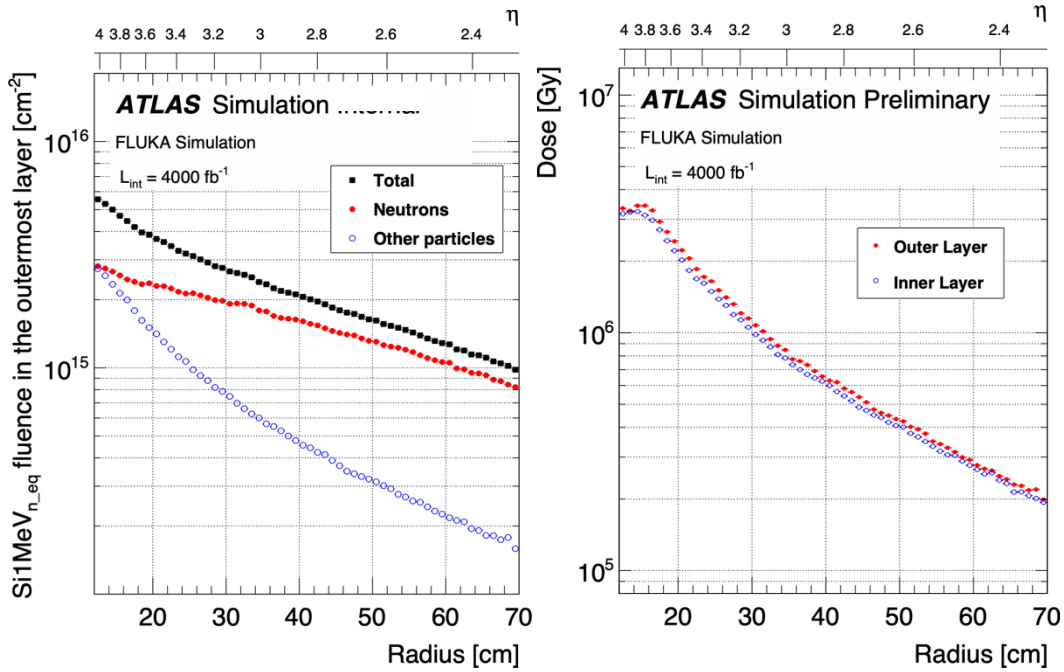

Fig. 4. (Left) Silicon 1-MeV-n_{eq} fluence only from neutrons (red circles) and Silicon 1-MeV-n_{eq} fluence from particles other than neutrons (open blue circles) for the outer silicon layer of the HGTD detector from r = 120 mm to r = 700 mm. (Right) Total dose in the inner (open blue circles) and outer (red circles) silicon detector layers of the HGTD from r = 120 mm to r = 700 mm. For both figures, the results correspond to the ATLAS FLUKA 3.1q7 geometry layout which includes the ITk geometry version Step 3.1 and the optimised moderator design between the endcap and the HGTD. The latter consists of a 50 mm BPE layer at r < 90 cm, continued with a 20 mm thick layer to the outer radius of the endcap. All results are scaled to the HL-LHC target integrated luminosity of 4000 fb^{-1} assuming an inelastic cross section of 80 mb. The pseudorapidity range shown on the top of each plot corresponds to the outer layer. Figures taken from [4].

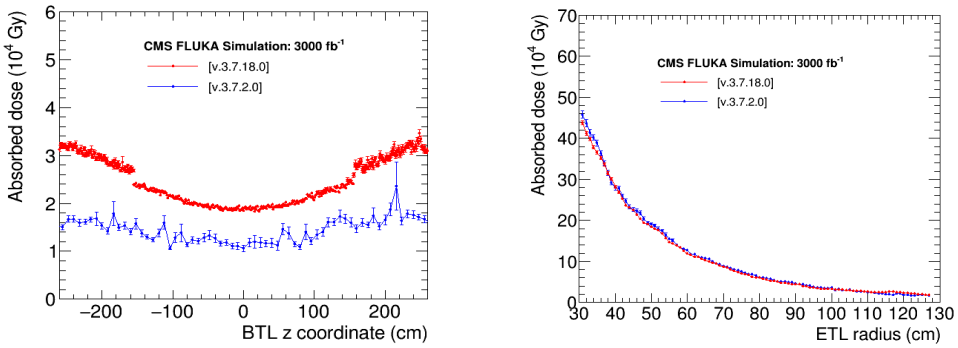

Fig. 5. Predicted doses in the BTL (Left) and ETL (Right) using the updated FLUKA CMS simulation v.3.7.18.0 (red) and the preliminary geometry model of the FLUKA simulation run v.3.7.2.0 (blue). Figure taken from [5].

The FCC-hh is a proposed hadron collider of the future. Figure 6 represents a simulation of that radiation environment; one sees that for an integrated luminosity of 30 ab^{-1} at center of mass energy 100 TeV, the innermost tracking detector will be exposed to as much as 10^{18} n_{eq}/cm^2 and 300 MGy at a rate of 10 GHz/cm^2 of charged particles. The forward calorimeters (representing a possible location for timing detectors) would see 5 x 10^{18} n_{eq}/cm^2 and 5000 MGy. As Figure 7 demonstrates, the effective pile-up (number of vertices compatible with reconstructed tracks) could, at the highest η region and without timing selections, reach values in the hundreds. The Conceptual Design Report (CDR) [6] for the FCC-hh notes that in CMOS 130 and 65 nm technologies, parasitic oxides used in the manufacturing process are responsible for significant degradation, and that although the 40 and 28 nm technologies' preliminary results show different phenomenology and slightly more promising radiation tolerance, "it is unlikely that circuits designed with these technologies could survive the TID levels (100-5000 MGy) expected in the inner tracker layers and the forward calorimeters." Furthermore, while it has been known for some time that TID limits the radiation tolerance of CMOS ASICs, these technologies have not been tested for displacement damage beyond a fluence of 5 x 10^{17} n_{eq}/cm^2, and that might lead to additional failure mechanisms. The CDR further notes that although CMOS technologies have been shifted from planar to bulk FinFETs starting from a nominal gate length of about 22 nm and have now reached the 7 nm pattern size, the literature [7] shows that TID tolerance has decreased with the miniaturisation due to radiation-induced leakage currents in the neck region of these devices, a characteristic that cannot be addressed by any design technique. Thus, construction of reliable electronics for FCC-hh detectors cannot simply rely on the improved radiation performance associated with miniaturisation.

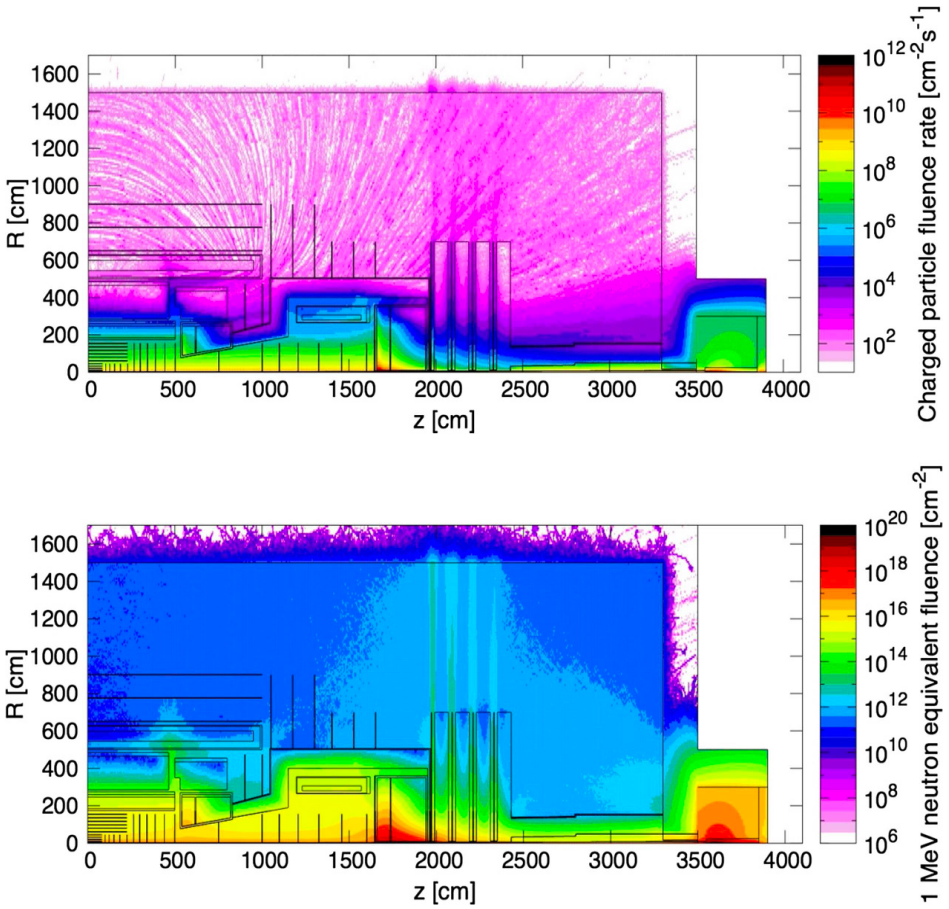

Fig. 6. Simulated radiation environment at a critical region of the FCC-hh. (Upper) Charged particle rate for L = 30 x10^{34} cm^{-2} s^{-1}. (Lower) 1-MeV neutron equivalent fluence for 30 ab^{-1}. Figure taken from [6].

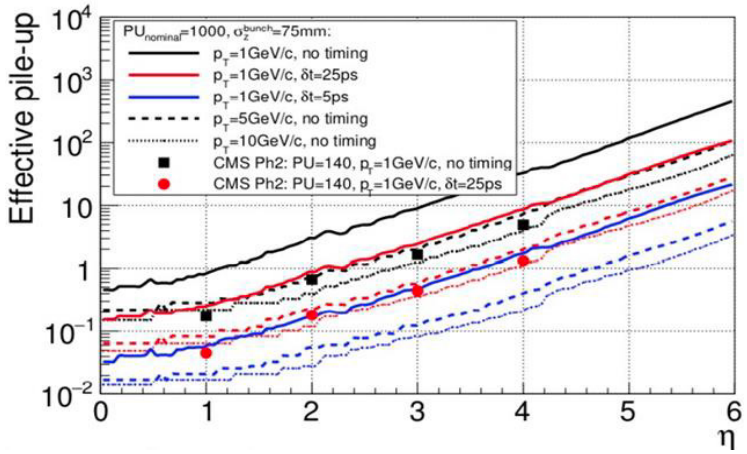

Fig. 7. Effective pile-up for different particle momenta at the FCC-hh. Figure taken from [6].

Vertex and timing detectors at future *lepton* colliders will confront extremes of TID as well as high energy hadron (HEH) effects, where the latter include single event effects (SEE) proportional to the fluence of hadrons with energies greater than 20 MeV, produced by ionisation by a single particle. SEE are characterized by their probability to occur; the effect depends upon the specifics of the device as well as the intensity and kind of radiation field in which it is immersed. Figure 8 shows the dose distribution in an FCC-ee arc half-cell. The results are normalized for 10^7 seconds of data and a beam current of 6.6 mA.

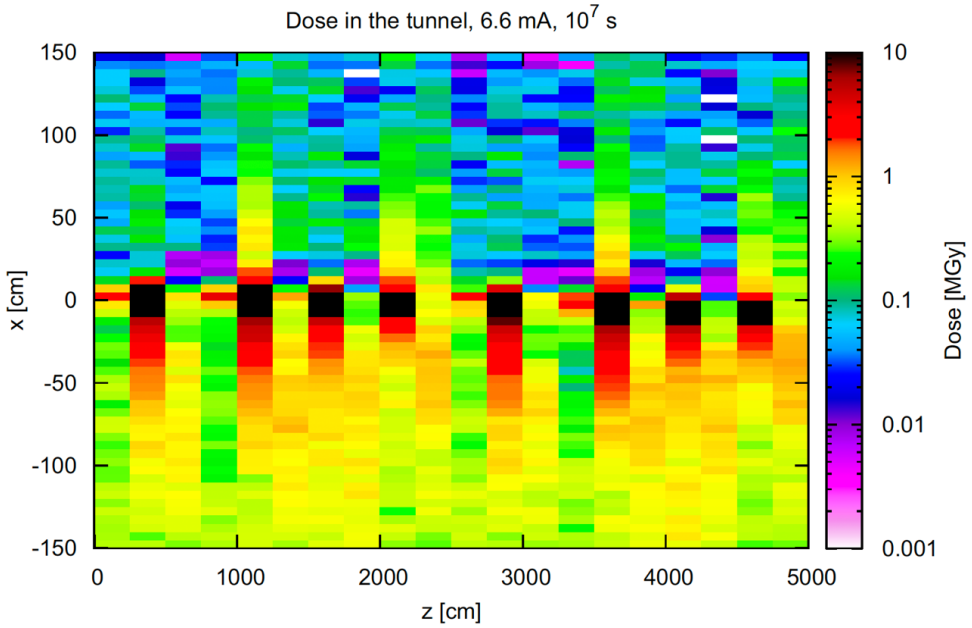

Fig. 8. The dose distribution in an FCC-ee arc half-cell. The results are normalized for 10^7 seconds of data and a beam current of 6.6 mA. Figure taken from [8].

In the case of the CEPC [9], also a proposed future lepton collider, for operation at the Z-pole energy, the annual dose at the first vertex layer is estimated to be 3.4 MRad, and the annual non-ionizing energy loss (NIEL) there, with a safety factor of 10, will be about 6.2 x 10^{12} n_{eq}/cm^2. Figure 9 shows the projected hit density, TID, and NIEL at different vertex layers due to pair production, off-energy beam particles, and the two combined.

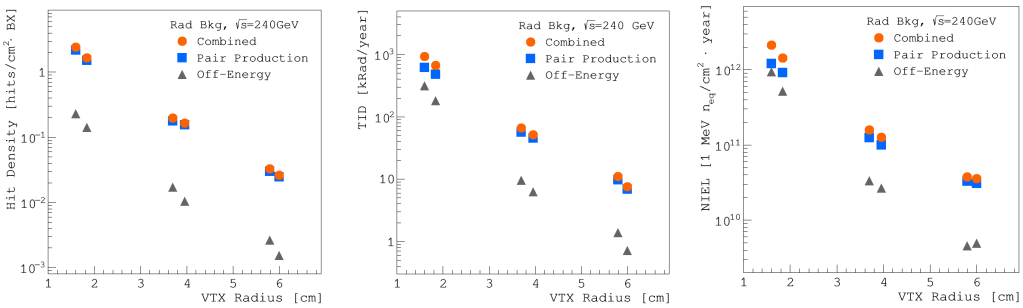

Fig. 9. (Left) Hit density, (Middle) total ionizing dose (TID), and (Right) non-ionizing energy loss (NIEL) at different vertex detector layers due to pair production, off-energy beam particles, and the two combined, for CEPC machine operation at center of mass energy 240 GeV. Figure taken from [9].

At CLIC [10], incoherent e^+e^- pairs will dominate the TID. NIEL damage in the barrel will be dominated by $\gamma\gamma \rightarrow$hadron events, while in the forward region, NIEL damage arises from a combination of incoherent e^+e^- pairs and $\gamma\gamma \rightarrow$hadron events. Table 1 shows the expected radiation damage for barrel pixel sensors and the lower end of the endcap pixel disks of the CLIC ILD detector concept. Safety factors for simulation uncertainties are not included; assuming an overall safety factor of two for the $\gamma\gamma \rightarrow$hadrons background and of five for the incoherent e^+e^- pairs, that simulation predicts a maximum exposure in the inner vertex layers of about 4 x 10^{10} $n_{eq}/cm^2/yr$ and up to 200 Gy/yr.

	Radius [mm]	Pairs NIEL [$10^9 n_{eq}/cm^2/yr$]	Hadr. NIEL [$10^9 n_{eq}/cm^2/yr$]	Pairs TID [Gy/yr]	Hadr. TID [Gy/yr]
VXB 1	31.0	3.87	11.51	39.43	4.57
VXB 2	33.0	2.88	8.57	27.83	4.01
VXB 3/4	44.0	0.99	4.60	8.01	2.46
VXB 5/6	58.0	0.45	2.92	3.30	1.66
VXEC 1/2	33.6	6.17	5.64	27.99	3.10
VXEC 3/4	33.6	6.72	5.79	29.25	2.96
VXEC 5/6	33.6	7.83	6.14	34.12	3.13

Table 1. Expected radiation damage (NIEL and TID) from incoherent pairs and $\gamma\gamma \rightarrow$hadrons for the barrel pixel sensors (VXB 1–6) and for the lower end of the endcap pixel disks (VXEC 1–6) of the CLIC ILD detector model. The numbers are quoted without safety factors for simulation uncertainties. Figure taken from [10].

Although radiation simulations at the ILC [11] show that the worst conditions are in the forward calorimeters, this report will restrict its attention to the vertex detectors. There, the beamstrahlung-induced background at the innermost layer leads to 1 kGy and 10^{11} $n_{eq}/cm^2/yr$. Components of this damaging flux include disrupted primary beam, bremsstrahlung photons, e^+e^- pairs from beam interactions, radiative Bhabhas, and $\gamma\gamma \rightarrow$hadrons or muons. This prediction assumes that neutrons backscattered from a beamdump are shielded. Table 2 summarizes expected damage in the various ILC detector concept vertex layers, predicted for center of mass energies of both 500 GeV and 1 TeV.

Sub-detector	Units	Layer	500 GeV	1000 GeV
VTX-DL	$hits/cm^2/BX$	1	6.320 ± 1.763	11.774 ± 0.992
		2	4.009 ± 1.176	7.479 ± 0.747
		3	0.250 ± 0.109	0.431 ± 0.128
		4	0.212 ± 0.094	0.360 ± 0.108
		5	0.048 ± 0.031	0.091 ± 0.044
		6	0.041 ± 0.026	0.082 ± 0.042

Table 2. Pair induced backgrounds in the Vertex Detector for nominal 500 GeV and 1 TeV collision energy beam parameters of the ILC. The double-layer option has been chosen for this simulation. The errors represent the RMS of the hit number fluctuations of approximately 100 bunch crossing (BX) simulations. Table taken from [11].

Radiation damage projections have also been initiated for a future muon collider. Figure 10, based on a FLUKA simulation, shows fluence in the range of about 10^{14} to 10^{15} $n_{eq}/cm^2/yr$ in the tracker and about 10^{14} $n_{eq}/cm^2/yr$ in the electromagnetic calorimeter - predictions that are comparable to those for the experiments at the HL-LHC.

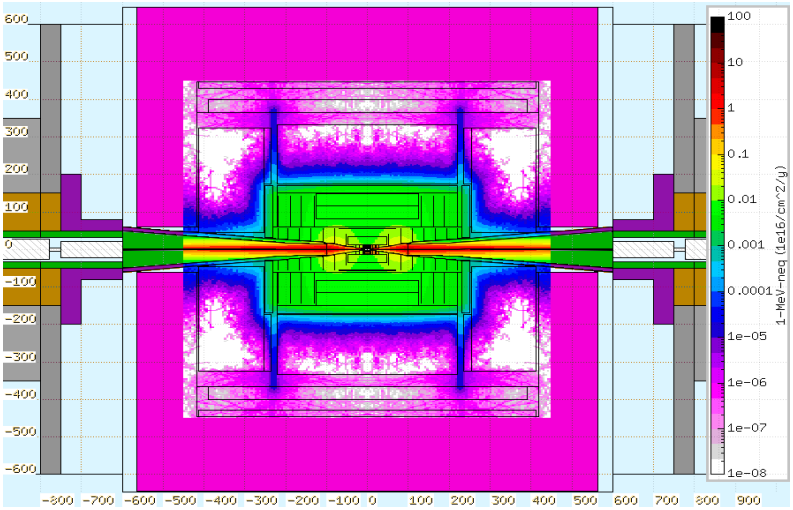

Fig. 10. Map of the 1-MeV-n_{eq} fluence in the detector region, shown as a function of the position along the beam axis and the radius of a muon collider detector concept. The map is normalised to one year of operation (200 days/year) and a collision rate of 100 kHz. Figure taken from [12].

The radiation environment at the Electron Ion Collider (EIC) has been predicted [13] using the BeAST detector concept for a location assumed at the RHIC IP6. At center of mass energy 140 GeV, for the highest e+p collision luminosity, which is 10^{34}/cm^2/s, the near-beamline prediction is about 2.5 kRad/year of TID in the backward arm calorimeters and over 10^{10} neutrons/cm^2/year in the vertex tracker and forward-backward calorimeters. The target radiation tolerance is established at 10^{15} n_{eq}/cm^2. The bunch crossing rate at the EIC will be less than 10 ns, necessitating fast timing detectors for these experiments. Figures 11 and 12 show the fluence and dose predictions respectively.

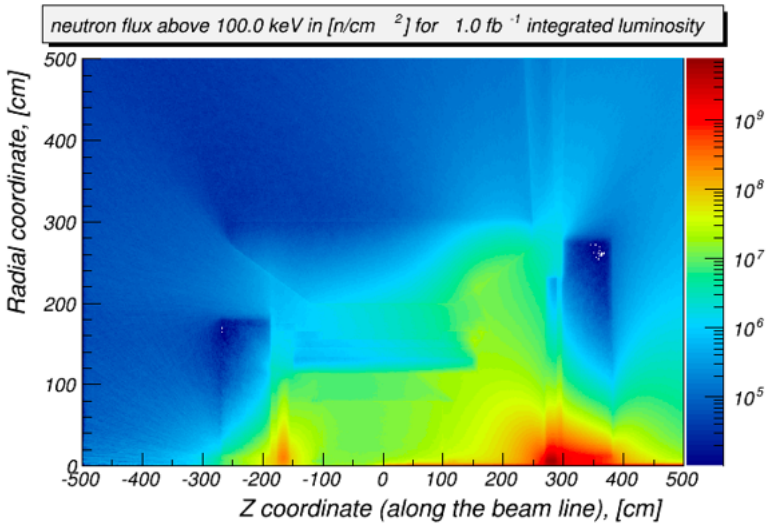

Fig. 11. Neutron flux from the e+p collisions at center of mass energy 140 GeV studied using the BeAST detector concept for the EIC with the assumed location in the RHIC IP6 experimental hall. Figure taken from [13].

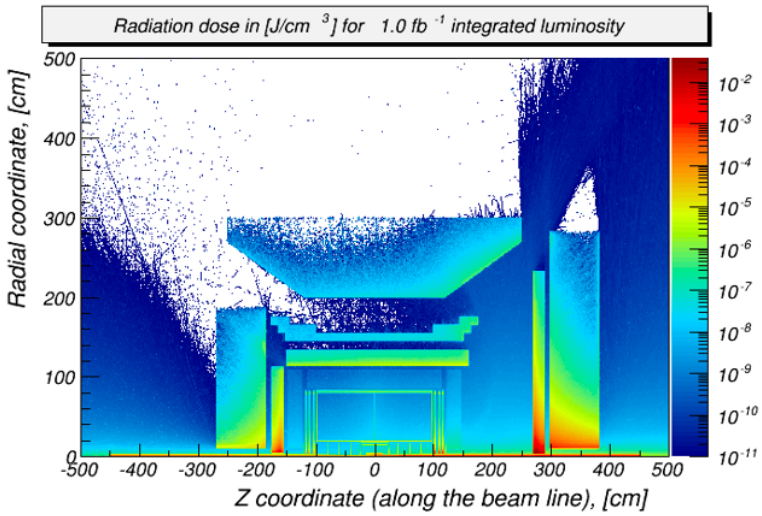

Fig. 12. Ionizing radiation energy deposition from e+p collisions at center of mass energy 140 GeV studied using the BeAST detector concept for the EIC. Figure taken from [13].

2. Challenges for vertex and track detection, and effects at the highest fluences

The detectors, whether for vertexing, timing, or "4D" in the radiation environments mentioned, must be able to maintain the quality of their response throughout the lifetime of operations. They must maintain adequate charge collection despite trapping, or they must inhibit the formation of traps. They must maintain adequate depletion volumes in which signal can form, because in under-depleted zones, the recombination time of the carriers falls exponentially with fluence. They must maintain an adequate signal-to-noise ratio despite development of damage-related leakage current. In the radiation field, detectors must maintain charge collection efficiency even as defects modify the space charge density; this has implications for the evolution of the power requirements. Detectors with built-in charge multiplication structures must maintain, despite radiation-induced acceptor removal, an acceptable level of gain and associated resolution. If, in detectors with internal gain, the signal diminishes with fluence, dynamical means to either increase the signal or decrease the noise must be possible, without loss of speed. A significant design consideration revolves around prevention of single event burnout, which involves irreversible breakdown and increases in probability as operating voltage rises.

The Hamburg Model [14], the Sheffield Model [15], and other parameter-based methods for predicting silicon sensor response to radiation damage, have been essential for detector studies since their release in 1999 and subsequently. These models need to be updated for the fluences foreseen today. One approach to this work is underway now in LHC experiment working groups using data from inner tracking detectors. A general model that starts from defect levels to describe macroscopic properties of silicon is very much needed and is one of the stated goals of the DRD3 Collaboration [16]. As input to these models, fundamental properties of the carriers, such as mobility and lifetime, must be quantified at the highest fluences.

However, some effects from radiation damage that are now being observed at LHC-level fluences are not extrapolating as badly as was previously expected. Trapping probability is

observed to saturate. A double junction emerges that leads to a deeper active volume than was anticipated. Controlled charge multiplication is seen to be achievable. All of this should be reflected with precision in the models.

3. Approaches to mitigation of damage effects, and opportunities

Trapping leading to signal loss is the issue of greatest concern for the vertex detector; and mitigation of acceptor removal is a research focus for the active gain devices. Several approaches are being employed: (1) reduction of the distance between electrodes; (2) incorporation of an amplifying structure into the device; and (3) application of defect engineering to the material. These are described in the following sections.

3.1 Reducing the drift distance

In planar devices, thin substrates inhibit trapping, and they have been shown to maintain charge collection even after being exposed to 10^{17} neutrons. As one example of the effectiveness of this approach, Figure 13 shows the mean charge recorded on a 75 μm epitaxial diode, integrating 3000 electrons under application of 1000 V bias after that exposure. It has been observed in this context that more charge is collected under forward bias than reverse, but that the signal-to-noise ratio under reverse bias is higher.

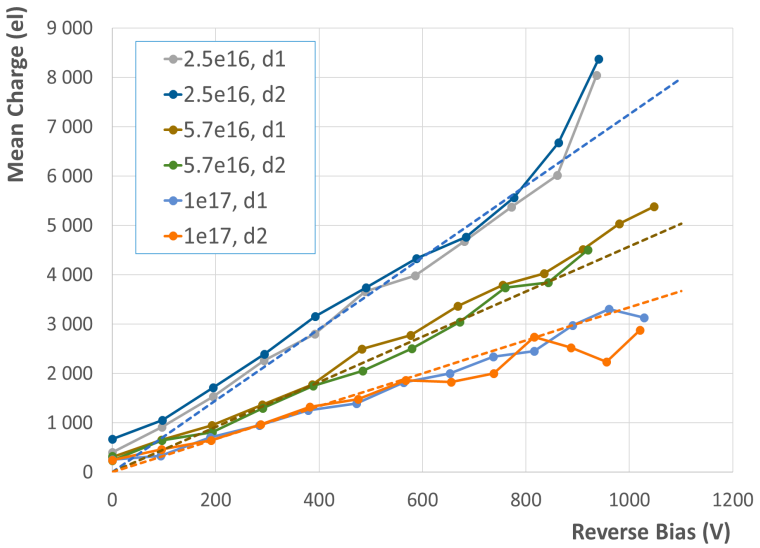

Fig. 13. Mean charge vs. bias voltage for reverse bias at different fluences for two devices per fluence. Dashed lines show the empirical formula provided in [17] fit to measurements. Figure taken from [17].

3D geometry, in which the electrodes penetrate the wafer vertically, is another approach. Here the depletion distance is decoupled from the wafer thickness. Inter-electrode distances below 25 μm are being produced, with corresponding pre-irradiation depletion voltages < 5V. Figure 14 illustrates the good efficiencies being observed for this technology at moderate bias voltages even after application of nearly 2 x 10^{16} n_{eq}/cm^2. Charge collection is modeled and observed for 3D devices beyond exposures of 10^{17} n_{eq} neutrons/cm^2 (Figure 15), and excellent timing resolution is being demonstrated (Figure 16) for them. The trench geometry is an evolution

of 3D that can smooth the electric field, preserving radiation tolerance associated with the small inter-electrode separation while improving the speed of signal collection. Figure 17 illustrates the classic trench, and Figure 18 the modified one. The simulation represented in Figure 19 illustrates the advantage trench geometry provides relative to cylindrical columns in signal collection time.

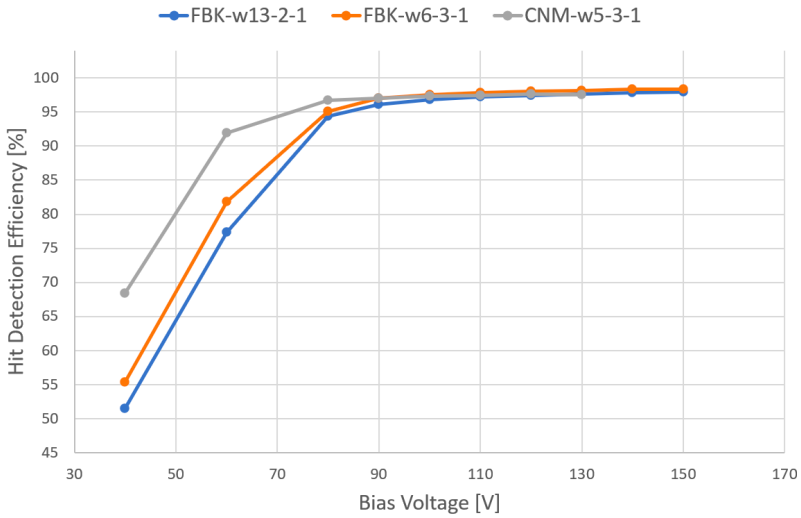

Fig. 14. Hit detection efficiency as a function of the bias voltage for three devices under test (DUTs). The pixel thresholds were tuned to an average value of 1000 electrons for all DUTs. The results refer to a region of interest with a uniform irradiation of 1×10^{16} $n_{eq}cm^{-2}$. The wZ-X-Y notation indicates the X-Y position of the sensor in the wafer Z of the production (either FBK or CNM). Figure taken from [18].

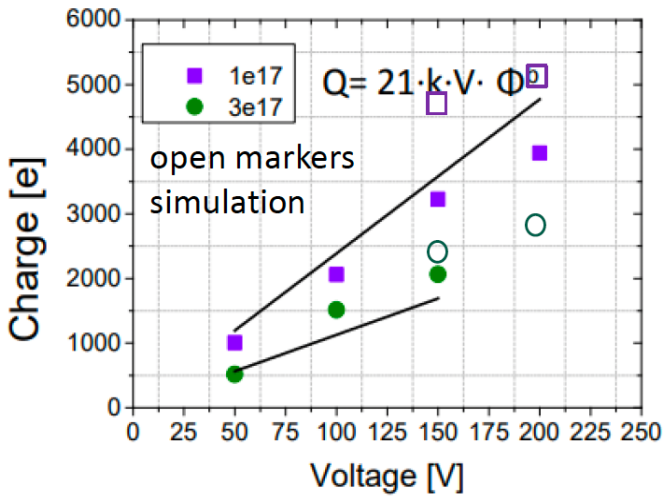

Fig. 15. Simulated and observed collected charge from 3D strip sensors irradiated with neutrons to FCC-hh fluences. Figure taken from [19].

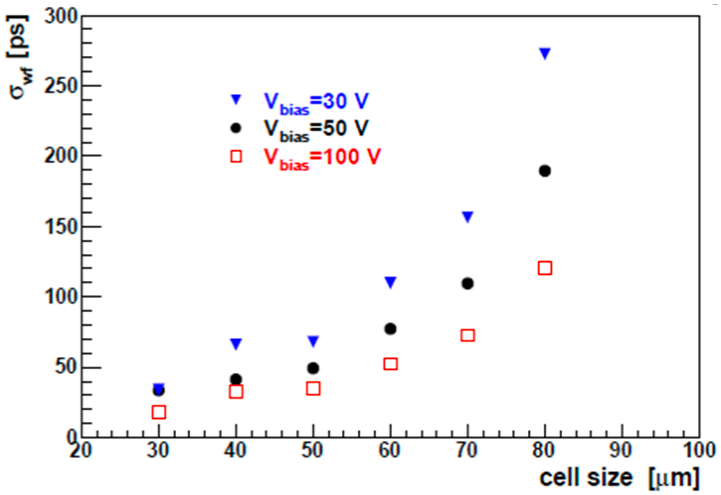

Fig. 16. Timing precision as a function of cell size for column 3D detectors with several bias conditions. Figure taken from [20].

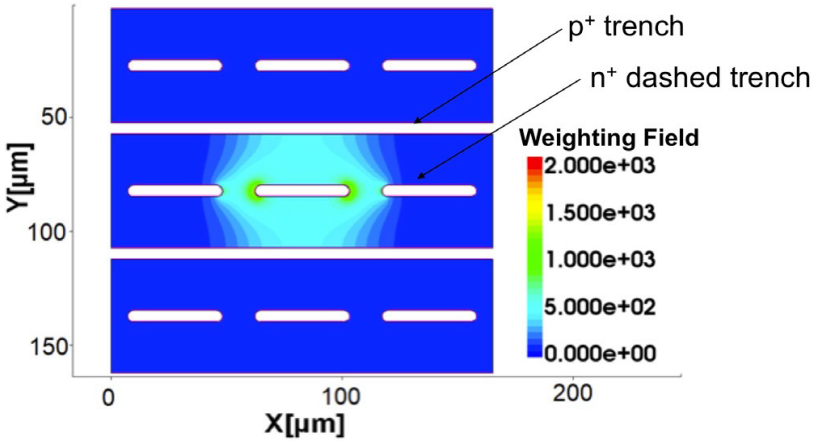

Fig. 17. Simulated model of the "classic" trench 3D pixel geometry. Figure taken from [21].

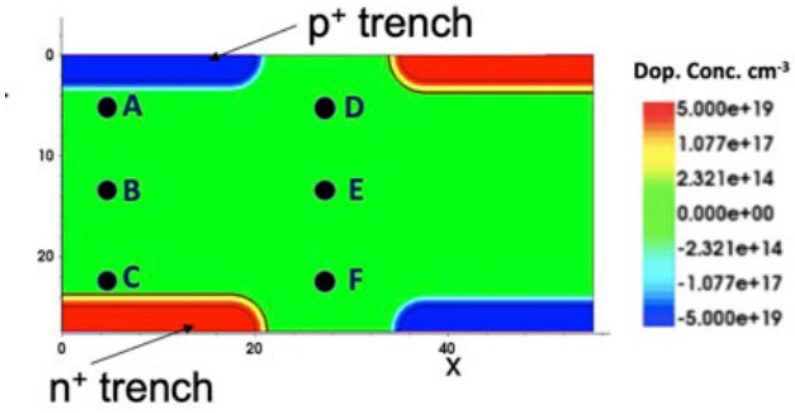

Fig. 18. Simulation model of the "modified" trench 3D pixel geometry. Figure taken from [22].

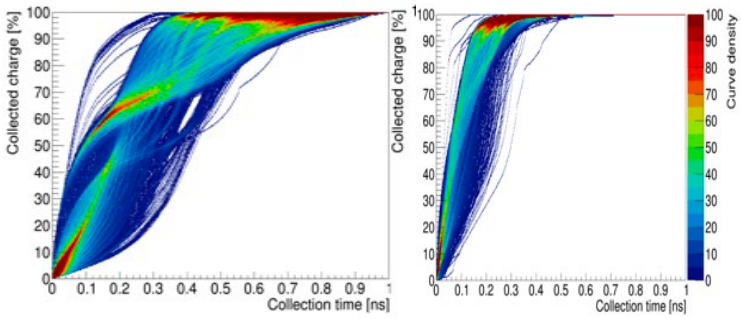

Fig. 19. Simulated charge collection curves for minimum ionizing particles uniformly crossing a pixel over its active area, in (left) a 5-column 3D geometry, and (right) a 3D trench geometry. Figure taken from [23].

3.2 Incorporating internal gain: low gain avalanche detectors

The DC-LGAD design [24] includes a shallow gain layer below the collection electrode, achieving gain for electrons but not holes, with a gain field of 300 kV/cm across ~1 micron near the junction. The bulk field is optimized at 20 kV/cm, for an electron drift velocity saturated at about 10^7 cm/s. Initial designs suppress breakdown by isolating the electrodes with p-stops combined with junction termination extensions (JTE) to reduce the electric field at the electrode edges. This provides amplification but diminishes the fill factor. A variety of solutions to increase the fill factor are being explored. Trench-isolated (TI) LGADs [25] replace the JTE with a silicon oxide-filled trench of width < 1 micron and depth a few microns. Deep Junction (DJ) LGADs [26] eliminate the JTE, pair a p^{++} gain layer with an n^{++} layer to lower the field, and bury the junction about 5 microns below the surface to maintain low fields at the surface. Sufficient gain is maintained although the field outside the electrodes is low. The inverse LGAD (iLGAD) [27] segments the p^+ electrode on the ohmic side and collects holes. In AC-LGADs, physical pixelation of the electrodes disappears [28]. The n^{++} implant at the junction is highly resistive and extends in a continuous sheet over the gain layer across the whole sensor. Application of a dielectric layer provides AC coupling to the readout.

Resistive Silicon Detectors (RSDs) are thin LGADs with resistive readout. The initial realization was AC-coupled [29]. Signal sharing occurs for charge induced in the resistive layer, and a fast signal is induced on the nearby AC pads. A spatial resolution better than $0.5 \times \text{pitch}/\sqrt{12}$ is achieved. DC-RSDs are now under development [30]: the oxide layer is removed and inter-pad resistors are added to confine the signal regions. That configuration avoids the AC-RSD problem associated with collection of leakage current only at the periphery and improves control of signal sharing.

With the goal to extend silicon LGAD operation up to 5 x 10^{17} n_{eq}/cm^2, the eXFlu [31] project is exploiting the saturation of damage effects that has been observed beyond 5 x 10^{15} n_{eq}/cm^2. This technology employs sensors of thickness limited to 20-30 microns, as these thin devices provide higher gain after irradiation. The design follows the "compensated LGAD" paradigm [32] in which the gain layer is constituted by a p- and n-doped combination. Before

irradiation, internal signal multiplication occurs in the gain layer; and as irradiation proceeds, the signal multiplication regime progressively moves from the gain layer into the bulk region.

3.3 Defect engineering

A next step for LGAD development utilizes defect engineering to inhibit acceptor removal. Active research involves carbon infusion, exploration of alternatives to boron as the primary dopant, and fine-tuning of the implant depth and geometry. In the technology known as half-activated boron [33], the device is doped with more boron than is required, so that atoms not incorporated into the silicon lattice are available to capture oxygen and suppress acceptor removal.

4. Goals and progress beyond silicon and beyond hybrid technology - a partial list

Exploration of the properties of wide bandgap semiconductors, including SiC and GaN, as well as diamond, is a contemporary research priority. Their high carrier saturation velocity predicts good operation in timing applications. The large band gap may permit operation without need for cooling. Illustrating development in this area, Figure 20 shows signal collection in SiC samples, where forward bias yields almost a factor of 10 increase in signal after exposure to 10^{15} n_{eq}/cm^2. Figure 21 demonstrates pulse height collection in a SiC sample after application of 1.1 x 10^{17} n/cm^2. Figure 22 shows the evolution of mean free path in diamond as a function of applied fluence up to nearly 6 x 10^{16} 24-GeV-p/cm^2.

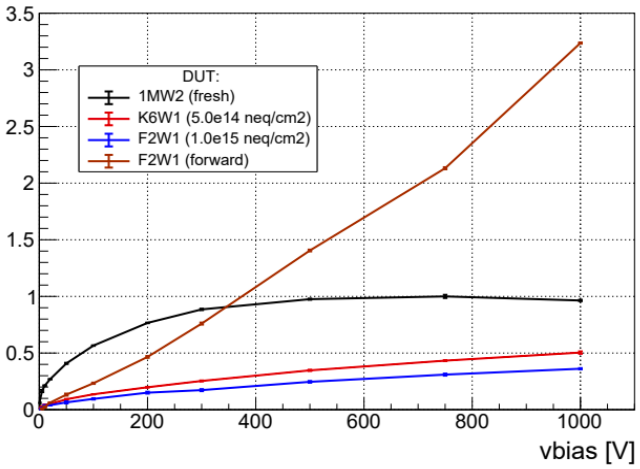

Fig. 20. Relative charge collection versus bias voltage for SiC diodes as a function of applied fluence and for forward and reverse bias conditions, normalized to the charge integral of the z-scan profile of the fully depleted unirradiated diode. Figure taken from [34].

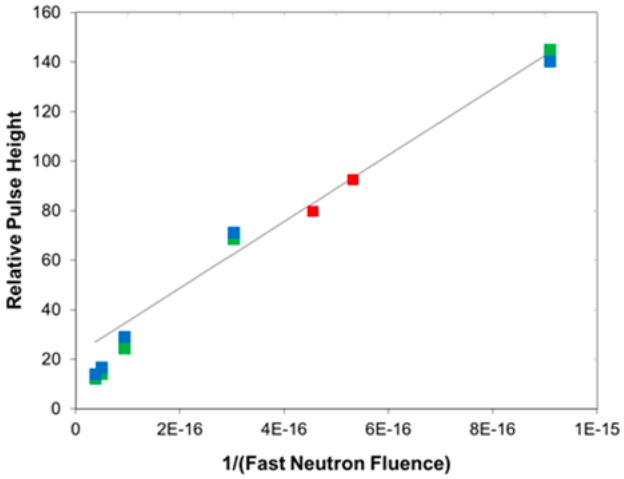

Fig. 21. ^{238}Pu pulse heights for SiC diodes exposed to fast neutrons. Pulse height is plotted as a function of reciprocal fast-neutron fluence. Figure taken from [35].

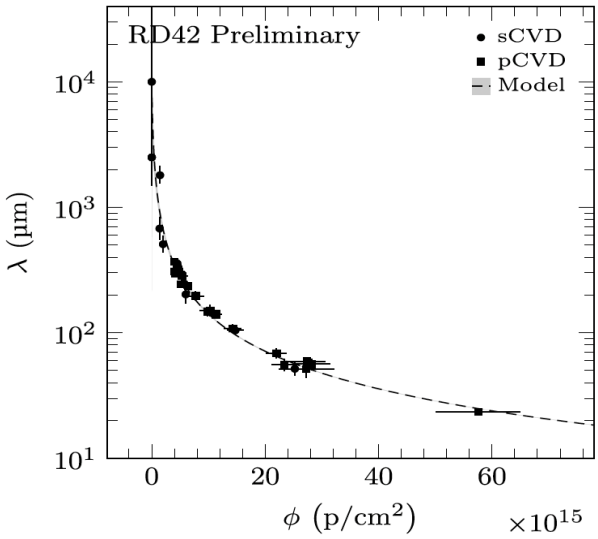

Fig. 22. Measured mean free path as a function of 24 GeV protons' equivalent fluence compared to the radiation damage model (dotted curve) described in Ref. 10 of [36]. Figure taken from [36].

The radiation hardness of monolithic active pixel sensors (MAPS) continues to improve, as is reflected in Figures 23 (for LF-Monopix2) and 24 (for MALTA2).

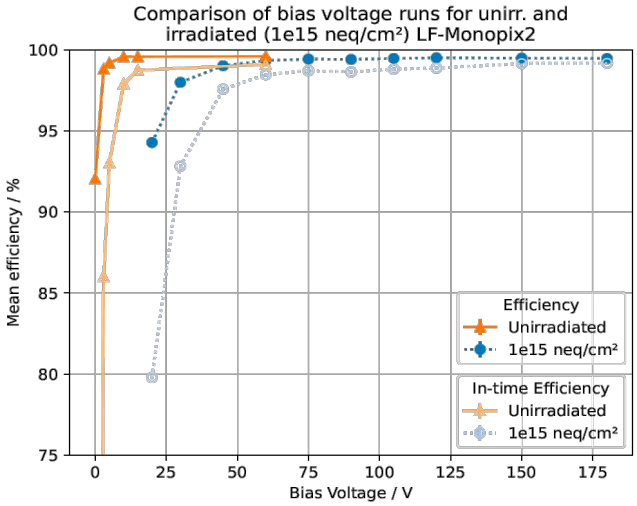

Fig. 23. Mean efficiency versus bias voltage for LF-Monopix2 devices unirradiated and after exposure to 10^{15} n_{eq}/cm^2. Figure taken from [37].

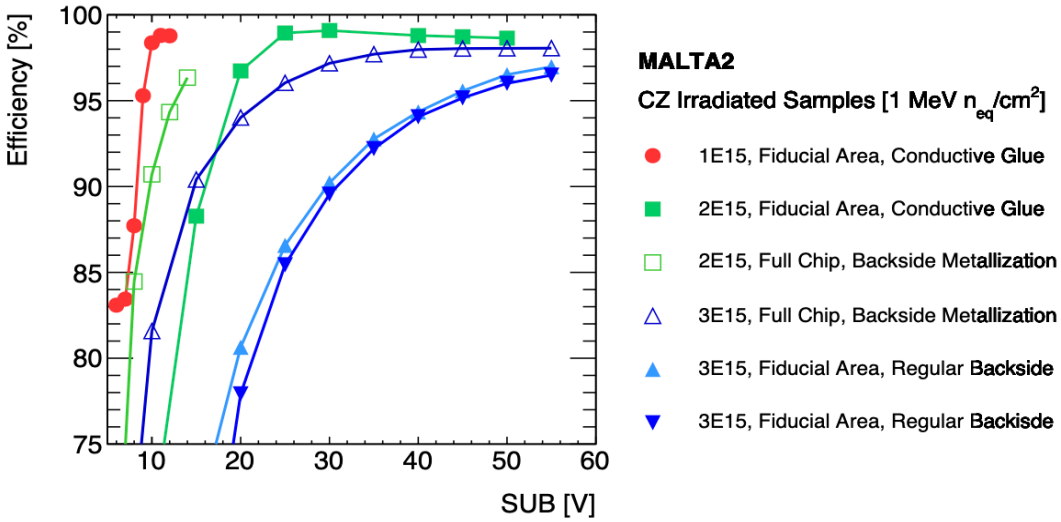

Fig. 24. MALTA2 Czochralski efficiency as a function of substrate bias voltage for neutron fluences from 1 to 3 x 10^{15} n_{eq}/cm^2 and various metalization options. Figure taken from [38].

Although this review has concentrated on sensor features, comparable evaluation needs to be applied to radiation tolerance in interconnects, mechanical supports, electronics, and services. Much work toward radiation tolerance in these areas is underway. Candidate materials are regularly evaluated directly in radiation environments, but their radiation tolerance is less often modeled. Guidance to particle physics may come from modelers in space science. References [39-41] offer interesting perspectives on radiation tolerant readout technologies, flexible printed circuit cables, and modeling of materials. Reference [39] discusses the radiation tolerance of silicon-photonic technology as a replacement for fiber-optical transceivers with their limitations.

5. Conclusions

Radiation environments are being carefully simulated for all future collider facilities envisoned. Saturation and non-linear effects are becoming apparent in silicon devices operated at the highest fluences. Trapping leading to signal loss is the primary challenge for the next detectors. However many ingenious technologies are being explored, and the future is bright.

References

[1] https://twiki.cern.ch/twiki/bin/view/AtlasPublic/RadiationSimulationPublicResults

[2] CMS Collaboration, *Technical Proposal for the Phase-II Upgrade of the Compact Muon Solenoid,* CERN-LHCC-2015-10.

[3] A. Ciccotelli et al., *Energy deposition studies for the Upgrade II of LHCb at the CERN Large Hadron Collider,* arXiv:2310.08281 [hep-ex].

[4] ATLAS Collaboration, *Technical Design Report: A High-Granularity Timing Detector for the ATLAS Phase-II Upgrade,* CERN-LHCC-2020-007.

[5] CMS Collaboration, *A MIP Timing Detector for the CMS Phase-II Upgrade: Technical Design Report,* CERN-LHCC-2019-003.

[6] A. Abada et al., *FCC-hh: The Hadron Collider: Future Circular Collider Conceptual Design Report Volume 3*, Eur. Phys. J. Special Topics 228, 755-1107 (2019).

[7] M.P. King et al., *Analysis of TID Process, Geometry, and Bias Condition Dependence in 14-nm FinFETs and Implications for RF and SRAM Performance,* IEEE Trans. Nucl. Sci. 64, no. 1, 285-292 (2017).

[8] A. Abada et al., *FCC-ee: The Lepton Collider: Future Circulat Collider Conceptual Design Report Volume 2,* Eur. Phys. J. Special Topics 228, 261-623 (2019).

[9] CEPC Study Group, *CEPC Conceptual Design Report: Volume II, Physics & Detector,* IHEP-CEPC-DR-2018-02.

[10] CLICdp members, *Physics and Detectors at CLIC: CLIC Conceptual Design Report,* CERN-2012-003, https://clicdp.web.cern.ch/content/conceptual-design-report.

[11] T. Behnke et al., eds., *The International Linear Collider Technical Design Report Volume 4: Detectors,* https://linearcollider.org/technical-design-report/.

[12] C. Accettura et al., *Towards a Muon Collider,* arXiv:2303.08533 [physics.acc-ph].

[13] R. Abdul Khalek et al., *Science Requirements and Detector Concepts for the Electron-Ion Collider: EIC Yellow Report,* BNL-220990-2021-FORE.

[14] M. Moll, *Radiation Damage in Silicon Detectors: Microscopic Defects and Macroscopic Properties,* Ph.D. Thesis, Hamburg University, 1999.

[15] R.S. Harper, *Radiation Damage Studies of Silicon Detectors and Searching for an Intermediate Mass Higgs Boson at ATLAS,* Ph.D. thesis, University of Sheffield, 2001.

[16] https://drd3.web.cern.ch/

[17] I. Mandic et al., *Measurements with silicon detectors at extreme neutron fluences,* 2020 JINST 15 P11018.

[18] R. Ceccarelli et al., *Results on 3D Pixel Sensors for the CMS Upgrade at the HL-LHC,* PoS Pixel2022 (2023) 046.

[19] M. Manna et al., *First characterisation of 3D pixel detectors irradiated at extreme fluences,* Nucl. Instr. and Meth. A 979 (2020) 164458.

[20] G. Kramberger, *Detectors for high radiation and extreme environments,* 12th Int. Conf. on Position Sensitive Detectors (2021), https://indico.cern.ch/797047/.

[21] R. Mendicino et al., *3D trenched-electrode sensors for charged particle tracking and timng,* Nucl. Instr. and Meth. A 927 (2019) 24.

[22] A. Boughedda et al., *A modified 3D-trench pixel detector: proof of concept by TCAD simulations,* Front. in Phys. 10 (2022) 957089.

[23] M. Garau, *Tests on radiation hardness of 3D-trench silicon sensors,* 18th Trento Workshop on Advanced Silicon Radiation Detectors, Trento 2023, https://indico.cern.ch/event/1223972/.

[24] G. Pellegrini et al., *Technology developments and first measurements of Low Gain Avalanche Detectors (LGAD) for high energy physics applications,* Nucl. Instr. and Meth. A 765 (2014) 12; H. F.-W. Sadrozinski et al., *Ultra-fast Silicon Detectors,* Nucl. Instr. and Meth. A 730 (2013) 226.

[25] G. Paternoster et al., *Trench-isolated low gain avalanche diodes (TI-LGADs),* IEEE Elect. Dev. Lett. 41, no. 6, June 2020.

[26] S. Ayyoub et al., *A new approach to achieving high granularity for silicon diode detectors with impact ionization gain,* arXiv:2101.00511[physics.ins-det].

[27] E. Curras et al., *Inverse Low Gain Avalanche Detectors (iLGADs) for precise tracking and timing applications,* Nucl. Instr. and Meth. A 958 (2020) 162545.

[28] G. Giacomini et al., *Fabrication and performance of AC-coupled LGADs,* 2019 JINST 14 P09004.

[29] M. Mandurrino et al., *Analysis and numerical design of resistive AC-coupled Silicon detectors (RSD) for 4D particle tracking,* Nucl. Instr. and Meth. A 959 (2020) 163479; M. Tornago et al., *Resistive AC-coupled silicon detectors: principles of operation and first results from a combined analysis of beam test and laser data,* Nucl. Instr. and Meth. A 1003 (2021) 165319.

[30] L. Menzio et al., *DC-coupled resistive silicon detectors for 4D tracking,* Nucl. Instr. and Meth. A 1041 (2022) 167374.

[31] https://aidainnova.web.cern.ch/thin-silicon-sensors-extreme-fluences

[32] V. Sola et al., *A compensated design of the LGAD gain layer,* Nucl. Instr. and Meth. 1040, 1 October 2022, 167232.

[33] S. Kita et al., *Improvement of timing resolution and radiation tolerance for finely segmented AC-LGAD sensors,* 18th Trento Workshop on Advanced Silicon Radiation Detectors, Trento 2023, https://indico.cern.ch/event/1223972/

[34] E. Curras et al., *Radiation tolerance study of neutron-irradiated SiC pn planar diodes,* 18th Trento Workshop on Advanced Silicon Radiation Detectors, Trento 2023, https://indico.cern.ch/event/1223972/.

[35] F. H. Ruddy, A. R. Dulloo and J. G. Seidel, *Study of the Radiation Resistance of Silicon Carbide Radiation Detectors,* Trans. of the Am. Nucl. Soc. 90 (2004) 348-349.

[36] N. Venturi et al., *Results on radiation tolerance of diamond detectors,* Nucl. Instr. and Meth. A 924 (2019) 241.

[37] I. Caicedo et al., *Characterization and radiation-hardness of the LF-Monopix2 DMAPS prototype,* 42nd RD50 Workshop, 2023, https://indico.cern.ch/event/1270076/.

[38] P. Allport et al., *Performance and radiation hardness of Tower 180 nm MALTA monolithic pixel sensors,* 18th Trento Workshop on Advanced Silicon Radiation Detectors, Trento 2023, https://indico.cern.ch/event/1223972/.

[39] M. Begel et al., *Readout Technologies for Future Detectors,* arXiv:2203.14894 [physics.ins-det].

[40] N.C. McFadden et al., *Radiation-tolerant, low-mass, high bandwidth, flexible printed circuit cables for particle physics experiments,* Nucl. Instr. and Meth. A 830 (2016) 461-465.

[41] N.E. Koval et al., *Modeling Radiation Damage in Materials Relevant to Exploration and Settlement on the Moon,* https://www.intechopen.com/chapters/81141.